



Auerswald, Matthias Marcus ; von Freyberg, Axel ; Fischer, Andreas

Laser line triangulation for fast 3D measurements on large gears

Journal Article as: peer-reviewed accepted version (Postprint)

DOI of this document* (secondary publication): <https://doi.org/10.26092/elib/3198>

Publication date of this document: 10/08/2024

* for better findability or for reliable citation

Recommended Citation (primary publication/Version of Record) incl. DOI:

Auerswald, M.M., von Freyberg, A. & Fischer, A. Laser line triangulation for fast 3D measurements on large gears. *Int J Adv Manuf Technol* 100, 2423–2433 (2019). <https://doi.org/10.1007/s00170-018-2636-z>

Please note that the version of this document may differ from the final published version (Version of Record/primary publication) in terms of copy-editing, pagination, publication date and DOI. Please cite the version that you actually used. Before citing, you are also advised to check the publisher's website for any subsequent corrections or retractions (see also <https://retractionwatch.com/>).

This version of the article has been accepted for publication, after peer review and is subject to Springer Nature's AM terms of use, but is not the Version of Record and does not reflect post-acceptance improvements, or any corrections. The Version of Record is available online at: <https://doi.org/10.1007/s00170-018-2636-z>

This document is made available with all rights reserved.

Take down policy

If you believe that this document or any material on this site infringes copyright, please contact publizieren@suub.uni-bremen.de with full details and we will remove access to the material.

Laser line triangulation for fast 3D measurements on large gears

Matthias Marcus Auerswald¹ · Axel von Freyberg¹ · Andreas Fischer¹

Abstract

The causes of geometrical deviations from the production process and the prediction of application properties, such as noise behavior, wear, or material fatigue, are only possible by having detailed information about the gear geometry. The gold standard for the gear quality inspection is represented by dimensional measurements with a tactile sensor system. As a result for industrial applications, the slow serial measurement leads to the compromise of a random inspection of the gear geometry. For the purpose of a faster and more extensive surface acquisition, a laser line triangulation sensor is investigated providing 1280 points at a line width of 25 mm with up to 200 lines/s. The results at the tooth of a large cylindrical involute gear with a pitch circle diameter of 922 mm and a face width of 246 mm show the qualification for fast three-dimensional measurements of the convex and reflective surface. The detection of the complete profile line at once is possible. It is shown that the measurement deviation of laser line triangulation can be minimized by increasing the dynamic threshold. The measurement deviations amount to $\pm 8.2 \mu\text{m}$ and can be attributed to random and systematic errors. Compared to the standard gear inspection, an acceleration factor of 5700 was attained. An optical scanning of the complete tooth flank provides the prerequisite for an identification of surface defects in the form of breakouts and blemish.

Keywords Large gear · Laser line triangulation · Geometric deviations · Quality inspection · Surface defects

1 Introduction

1.1 Motivation

Large cylindrical involute gears with a pitch circle diameter of 922 mm, a face width of 246 mm, and a module of 10 mm (Fig. 1) are used, e.g., for gear boxes of wind turbines and industrial vehicles and large gear standards. In Germany, more than 27.000 wind turbines are installed [1]. In this context, insurance statistics reveal that gearbox damages cause about 20% of the possible damages and disturbances to a wind power installation [2]. One reason that the gearboxes do not reach the planned service life is the combination of large and changing loads with lightweight design requirements. Thus, for large gears which are used under high-demanding conditions, e.g., in gearboxes of wind turbines, a more extensive

inspection is recommended. The prediction of application properties, such as noise behavior, wear, or material fatigue, and the causes of geometrical deviations from the production process are only possible by having more detailed information about the large gear geometry (Fig. 1).

Manufacturing gears is a key technology, and the quality inspection of gears is carried out under well standardized directives [3]. But, there is a growing inspection demand for the measurement of large gears, which differs from the requirements known for smaller gears due to different production processes [4]. Smaller automotive gears are often completely machined in less than 1 min. In contrast, the production processes for large gears consist of more steps and can last several hours. The temperature behavior of the machine tool and tool wear differs fundamentally and induces heat in parts of the workpiece. For small gears, the induced heat is minimal and almost symmetric. Due to the short cycle time, tool wear and thermal drift of the production machine can be neglected when considering a single part. In contrast, for large gears, the latter two factors have to be taken into account during production processes as well as in the measurement strategy during quality control. In addition, the production processes are often characterized by a non-symmetric heat induced in the part due to other milling or grinding strategies. Thus, it cannot be

✉ Matthias Marcus Auerswald
m.auerswald@bimaq.de

¹ Bremen Institute for Metrology, Automation and Quality Science (BIMAQ), University of Bremen, Linzer Str. 13, 28359 Bremen, Germany

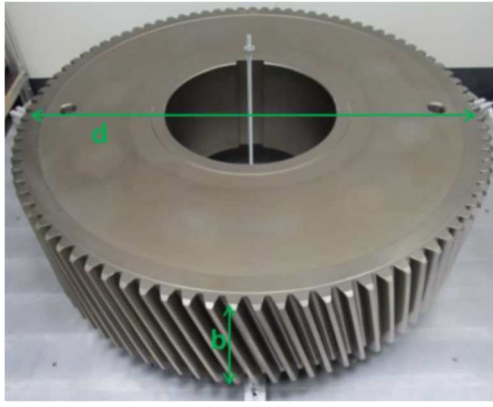


Fig. 1 Large cylindrical gear with a pitch circle diameter $d = 922$ mm, a face width $b = 246$ mm, and a module of 10 mm

assumed that all teeth of the gear nearly have the same shape and surface characteristics. For more detailed assessment of the quality of large gears, a comprehensive and multidimensional inspection is required [5].

1.2 State of the art

Gear measuring instruments (GMI) and coordinate measuring machines (CMM) with a tactile sensor system represent the gold standard for the quality testing of gearings, and CMMs are offered in different designs [6]. Furthermore, for the assessment of runout and radial composite deviations, special measuring devices for double-flank composite action tests are used. Modern CMMs of portal, bridge, or stator construction are recommended for large components, whereas CMMs of the bridge design are recommended for gear testing and reach measuring volumes of $6.0 \times 4.5 \times 3.0$ m³. The determinants for involute cylindrical gears and their deviations are defined in the standard [6]. The tolerances for large gears start for the gear quality 5 at almost one hundredth of a millimeter [6]. The evaluation of these tolerances places high requirements on the measurement technique [4, 7] that the standardization renounces compliance with the golden rule of the measuring technique. The standard gearing test consists of the measurement of one profile and one flank line on 3–4 teeth of the gear [8]. A single measuring point is additionally recorded on each tooth for evaluating pitch and runout deviations [6]. This spot-check represents a compromise between measurement time and information content and is justified by the fact that tactile measurement methods are used without exception in industrial practice. This hinders in particular the multidimensional inspection of large gears while the demands are continuously increasing.

However, the development of large gear standards started only a few years ago [9] and corresponding calibration standards for gears with a diameter of more than 1 m are not commercially available. The verification of the geometry in the standard tactile gear inspection is insufficient to improve

the quality of large gears [4, 5], because the detection of the tooth geometry with tactile measuring systems is very time-consuming and also exorbitant in practice. Goch et al. came to the conclusion that hardly any improvements in the development of tactile measurement technology are to be expected [3]. CMMs are designed to perform only single measurements from a specified direction at a given time. This serial data acquisition with a single measurement point leads to an increased measurement time, in particular for large components such as a large gear (Fig. 1). Hence, a comprehensive quality assessment under economic aspects can only be carried out by faster optical sensors in combination with measurement concepts for parallel multi-point acquisition.

For the area of large volume metrology (LVM), conventional coordinate measuring are used less. In this area of measurement technology, the paradigm is to bring the measuring system to the object and not conversely [10]. In the field of production technology and thus the area of large gears, LVM measurement tasks often require a large dynamic range of the measuring system [11]. In the context of the requirements for a large dynamic range, short measuring time, and the logistical effort, there are great challenges.

At tactile sensors with optical signal processing, a probe ball is guided to the measuring object and the lateral deflection is determined by image processing via telecentric optics [12]. This measuring system is especially used for the measurement of very small components and micro-gearings. An acceleration of large gear measurements cannot be achieved with this principle. Under certain boundary conditions, the measurement of the contour of spur gearings is possible with image processing sensors [13]. But this measuring principle is only suitable for straight and narrow gearings. The point-by-point detection of coordinates by an interferometric probe system based on frequency modulation is presented in [14]. Due to the serial data acquisition, this sensor offers only low speed advantages. In addition, the movement axes of a large CMM are required, which means a corresponding technical effort. Optical gear measurement approaches, which are area-oriented, are not accurate enough for the general gear quality inspection task, or they are only suitable for special applications, like stripe pattern projection on forged gears [15]. For an optically flat measurement, an approach has been published which can detect an interference pattern of a tooth flank on the basis of an interferometric system using phase shift technology [16]. The measured interference pattern corresponds to simulated data, but no statement was made about quantitative deviations or the measurement uncertainty that can be achieved. Moreover, there are further optical measuring principles, e.g., fiber optic distance sensors [17], confocal microscopy, chromatic confocal distance measurement, or hybrid systems such as chromatic confocal spectral interferometry [18]. In particular, axial measurement principles such as the chromatic confocal principle, transit time method [19], or

autofocus sensors are suitable to implement a scanning process to detect the surface [20]. However, such measuring systems have not been investigated in detail for the usage of large gear metrology so far.

For a reduction of the measuring times and an increase of the information density, triangulation methods with structured illumination are far more suitable [21]. According to [3, 22], the triangulation principle enables kilohertz data rates even for the linear multi-point measurement in parallel, and it is considered to be suitable for the measurement of gears and the detection of tooth flanks. But the required measurement uncertainty is not achieved to evaluate the tolerances of the tooth deflections and for the special case of optically cooperative surfaces. However, the results do not disprove the basic suitability of laser triangulation for gear measurements. An advantage of laser triangulation is that it can be implemented point-by-point, line wise [23] and even in the form of stripe pattern projections [24] or fringe reflection photogrammetry [25]. Depending on the implementation, a high data rate is possible and the measuring systems are quite insensitive to vibrations [26]. Today, laser line scanners, i.e., laser line triangulation sensors, are frequently used as an alternative for tactile probes on CMMs. In comparison to tactile probes, the main advantages are to measure without being in contact with the gear and also to capture many points in a short period of time. However, optical geometrical measurements of large gears face a lot of challenges, which differ from the requirements known for small gears. The combination of reflective and convex surfaces, limited accessibility (see Fig. 2), and the area of large volume metrology represent a challenge for precise geometrical measurements with optical sensors on large gears.

In particular, a high dynamic range is necessary since the deviation of the considered large gear shows a proportion of 10^{-5} of the diameter (compare Table 1). For large cylindrical gears, the principle of laser triangulation has not been adequately tested, yet. An open question is whether a fast detection of convex and reflective three-dimensional surfaces of the tooth flank (Fig. 2) of large cylindrical gears (Fig. 1) with a helix angle of 15° is possible by using a laser line triangulation sensor. Furthermore, the question arises whether this can increase the data rate and what is the resulting measurement deviation?

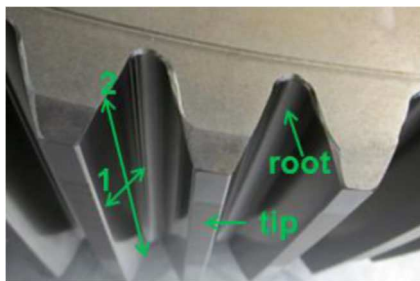


Fig. 2 Surface profiles on a tooth flank in profile (1) and helix direction (2)

Table 1 Comparison of gear parameters and tolerance (according to ISO1328-1) of large and small gears

	Large gear	Small gear
Diameter, d	955 mm	68 mm
Weight, m	1.100 kg	0.5 kg
Total profile deviation, F_α	16 μm	6 μm
Module, m	10.0 mm	1.7 mm
Number of teeth, z	89	33
Pressure angle, α	20°	16°
Helix angle, β	-15°	33°
Face width, b	246.0 mm	17.3 mm

1.3 Aim and outline of the article

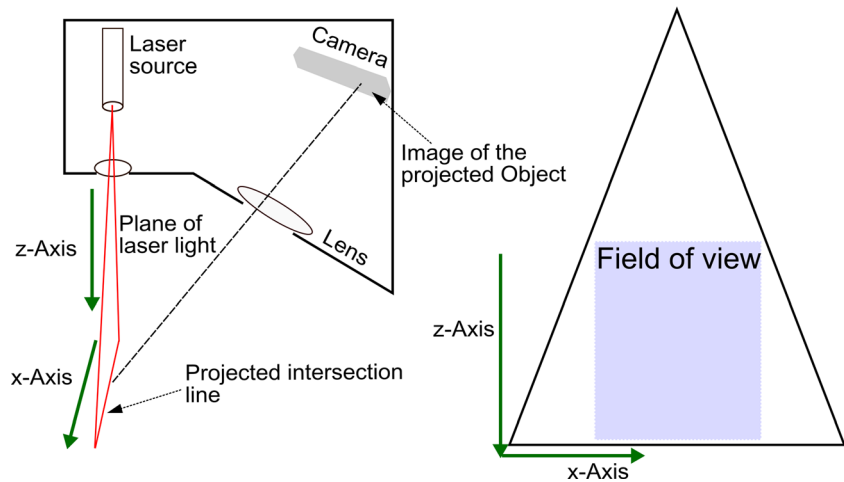
The aim is to investigate the line-orientated detection of convex and reflective surfaces of large cylindrical gears (Fig. 1) by applying laser line triangulation. For this purpose, the measurement setup and the geometric model and evaluation strategy are described in Sections 2 and 3. Moreover, the three-dimensional detection of the complete surface of the tooth flank by a linear scanning with the sensor is examined. In this context, the aim is the detection of surface defects in form of breakouts and blemish. The experimental results are verified and validated in Section 4. The article closes with the conclusions in Section 5.

2 Measurement principle

The setup of the laser line triangulation (LLT) is depicted in Fig. 3 a. Such a laser line scanner is used as an optical sensor system for the fast acquisition of the surface profile of a tooth flank, e.g., the profile and the helix as well as the tip and root of the tooth (Fig. 2). The LLT use the principle of triangulation for two-dimensional profile detection on different target surfaces. The principle of triangulation is based on the Scheimpflug principle [27, 28].

By using special lenses, a laser beam is enlarged to form a static laser line that is projected onto the surface. The diffuse reflected part of the laser light from the object is imaged over a lens optic on a highly sensitive sensor matrix. Through calibration of the scanner, the camera coordinates are linked with the coordinates in the plane of the laser light. Since the dimensions of the camera are limited, the scanner will also have a limited field of view (Fig. 3b). In addition to the distance information (z -axis), the controller also uses this camera image to calculate the position along the laser line (x -axis). These measured values are depicted in a two-dimensional sensor coordinate system (SCS) that is fixed with respect to the sensor. In the case that the sensor is traversing over the surface with a constant distance, it is possible to obtain 3D measurement values.

Fig. 3 Laser line triangulation. **a** Measurement principle. **b** Resulting field of view in the sensor coordinate system (x, z)



3 Experimental method

The challenges at large cylindrical gears are unfavorable surface properties, like convex and reflective surfaces, which are also difficult to access (Fig. 2). Furthermore, the application field of large volume metrology is also a great challenge because of the increased dynamic range of the measurement system. Table 1 shows the comparison of gear parameters and tolerances according to ISO1328-1 in comparison between a large and a small gear.

With regard to the diameter of the gearing, a measurement uncertainty is necessary for the evaluation of the total profile deviation F_α of large gears, which must be smaller by one order of magnitude than in the case of small gears. Especially difficulties in handling and clamping the large gear, their deformation due to gravity and the temperature behavior, as well as the lack of appropriate calibrated gauges necessary for a traceability of measurements have to be mentioned. The listed aspects before are currently not considered. Only the line-orientated detection of convex and reflective surface of large gears and three-dimensional detection of the complete surface of the tooth flank by a scanning process is considered.

For tactile measurements, the information of the surface normal vector comes from the probe head deflection and is important for the evaluation of the deviations of the gear. In the case of geometric measurements with the LLT (2.5-D areal sensor), there is no direct information about the surface's normal vector for each measurement point. Other main influence factors, i.e., the acceptance angle and the working distance of the LLT sensor, have to be taken into account for the measurement on large gears and the evaluation of deviations. The fact that the above parameters cannot be assumed to be constant during the measurements with the LLT, because they also depend on the surface quality of the gear, represents a non-negligible issue.

Additionally, the evaluation process for gear measurements with LLT have to take care of outliers and they have to deal with missing points and a varying point density and distribution.

The solution for evaluating optical measurement data is achieved by a model-based evaluation which is described in Section 3.1. The experimental setup and the alignment of the LLT sensor for measurements on large gears is shown in Fig. 4. The investigated gear is shown in Fig. 1, and the geometrical parameters of the gear are listed in Table 1.

The light source of the LLT sensor consists of a semiconductor laser with a wavelength of $\lambda = 658$ nm, and the sensor matrix has a size of $1280 \text{ pixel} \times 1024 \text{ pixel}$. It has a resolution of 1280 points at a line width of 25 mm. The profile frequency depends on the required exposure time, but the maximum is 200 lines/s. The trapezoidal field of view (cf. Fig. 3b) of the image matrix is 25 mm in x -direction and 25 mm in z -direction. The basic distance of the sensor from the gear amounts to 53.5 mm.

The assembly of the LLT for the detection of a complete tooth side is shown in Fig. 4. The detection of the complete tooth side is realized by a traversing process of the LLT sensor. The traversing process is done by a vertical linear axis, which is positioned by a stepper motor which allows the continuous movement of the sensor. Due to the measuring range of the LLT sensor of 25 mm, the helical surface of the tooth of a running gear remains in the measuring range of the sensor. Exceptions are given for certain ratios of the face width and helix angle as in the case of worm wheels. The scanning process is ensured along the face width of the gear, whereby the direction of the scanning takes place from the top to the bottom.

3.1 Geometric model and evaluation

The target geometry of the involute of large gears can be geometrically constructed according to Fig. 5 with the data

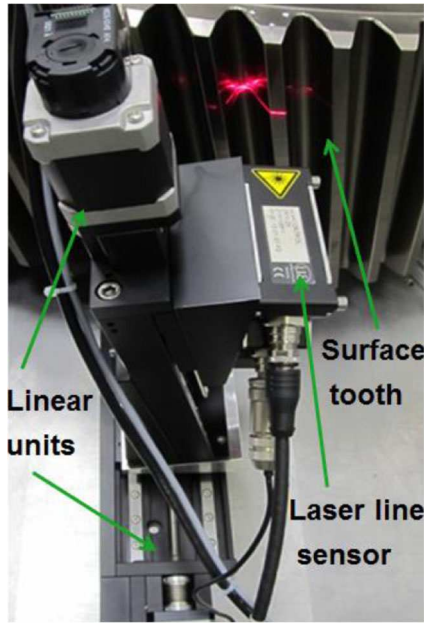


Fig. 4 Alignment of the laser line scanner to the gearing

listed in Table 1. The coordinates (x', y') of the i -th point P'_i on a flank of a large gearing can be calculated as follows in the workpiece coordinate system (WCS) according to [3, 29]

$$P'_i = \begin{bmatrix} x'_i \\ y'_i \end{bmatrix} = \vec{a} + \vec{b}$$

$$= r_b \cdot \begin{bmatrix} \cos(\xi_i + \vartheta_z - \psi_b) \\ \sin(\xi_i + \vartheta_z - \psi_b) \end{bmatrix} + r_b \cdot \xi_i \cdot \begin{bmatrix} \cos\left(\xi_i + \vartheta_z - \psi_b - \frac{\pi}{2}\right) \\ \sin\left(\xi_i + \vartheta_z - \psi_b - \frac{\pi}{2}\right) \end{bmatrix} \quad (1)$$

The vectors \vec{a} and \vec{b} define the radial and tangential direction, respectively, ξ_i is the rolling angle, ϑ_z determines the position of the centerline of tooth z , and ψ_b is the tooth

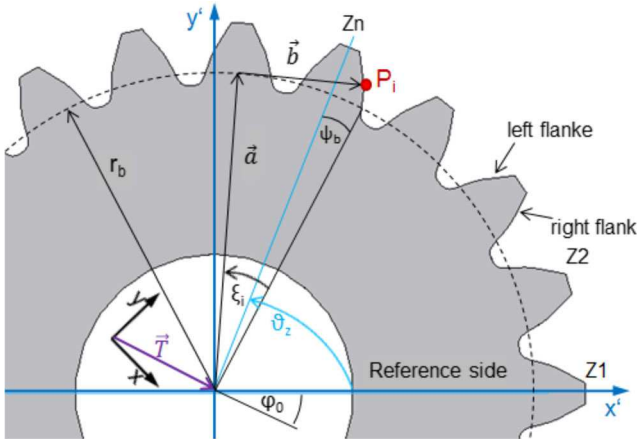


Fig. 5 Geometric construction and relationship of a measuring point on the involute flank of a tooth z in the workpiece coordinate system (x', y')

thickness-half-angle at the root circle with radius r_b . For calculating the coordinates

$$P_i = \begin{bmatrix} x_i \\ y_i \end{bmatrix} = r_b \cdot \begin{bmatrix} \cos(\xi_i + \vartheta_z - \psi_b + \varphi_0) \\ \sin(\xi_i + \vartheta_z - \psi_b + \varphi_0) \end{bmatrix} + r_b \cdot \xi_i \cdot \begin{bmatrix} \sin(\xi_i + \vartheta_z - \psi_b + \varphi_0) \\ -\cos(\xi_i + \vartheta_z - \psi_b + \varphi_0) \end{bmatrix} + \vec{T} \quad (2)$$

within the measurement coordinate system (x, y) , the translation vector $\vec{T} = [x_t, y_t]^T$ and the angle ϕ_0 are integrated into Eq. 1. Different preliminary works [29, 30] are the basis for the evaluation of the individual surface profile line (measuring points) of a tooth flank. By the calculation of the distances between the measuring points to the target geometry, the measurement data can be transformed into the WCS. The orthogonal distance d_i of a measuring point P_i from an involute in the transverse plane

$$d_i = r_b \cdot \left(\sqrt{\frac{r_m^2}{r_b^2} - 1} - s \cdot \left(\arctan\left(\frac{y_m - y_t}{x_m - x_t}\right) - \vartheta_z + \psi_b - \varphi_0 + \arctan\left(s \sqrt{\frac{r_m^2}{r_b^2} - 1}\right) \right) \right) \quad (3)$$

can be directly calculated according to [31]. Here, s indicates a flag which is -1 for a left flank or $+1$ for a right flank, respectively, and

$$r_m = \sqrt{(x_m - x_t)^2 + (y_m - y_t)^2} \quad (4)$$

is the radius of the measured point in polar coordinates within the WCS. The orthogonal distances of the measured points will be calculated according to Eq. 3 based on the corresponding parameters of the large gear (Table 1). Thereby, the measured points can be transformed into the WCS. The evaluation in Section 4.2 focuses on the evaluation of shape deviations of the involute flank and can be expanded to the calculation of standard profile and helix deviation parameters. Remaining quality parameters, such as the pitch deviation (F_p) or the runout deviation (F_r), require a synchronized angle measurement between the gear and the LLT. This is not given in this arrangement, and, therefore, the estimation of those parameters is not subject of this paper.

4 Results

4.1 Time resolution and measuring rate

Figure 6 shows all measurement points which are detected in the field of view of the sensor. The measuring frequency is

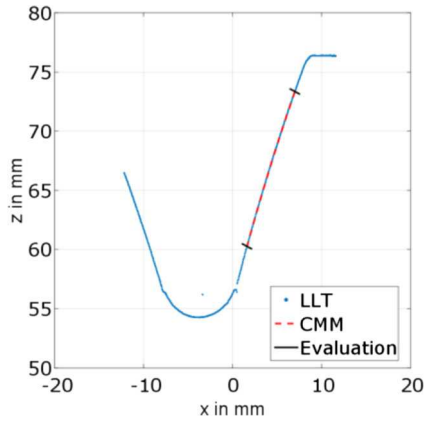


Fig. 6 All measurement points of one single shot from the LLT in the sensor coordinate system (x, z) compared to the transformed CMM measurement points within the evaluation range

200 Hz (5 ms) for 1280 measurement points, which are detected simultaneously. Despite the convex and reflective surface shape, the detection of almost the complete surface profile line of a tooth flank from the tip to the root is possible in one shot, cf. Fig. 6.

From the profile line, the region of interest is extracted for the subsequent evaluation of the involute. In the experimental investigations, it could be observed that the orientation of the sensor has a direct influence on the appearing of multiple reflections and the number of valid measurement points. According to the measurement results shown in Fig. 6, a region that cannot be detected is located in the root area at $x = 1$ mm. The reason is that undercuts, artifacts arise and multiple reflections due to the steep viewing angle of the sensor to the surface of the involute. In addition, the optical axis of the laser source is oriented in the transverse section of the large gear. However, the missing region is negligible since it is not important for the functional inspection of a gear. The projection of the laser line in the root area leads to multiple reflections, but the multiple reflections can be minimized by the usage of a respective aperture, which is attached at the tooth tip. The residual points that remain after such minimization are not taken into account in the evaluation, because these points are outside of the selected evaluation range (compare Fig. 6). The applied method for the geometric model and evaluation (Section 3.1), which uses the sum of the least squares of the orthogonal distances, allows at the same time the implantation of an outlier test according to Grubbs [32]. As a result, a certain number of outliers, which might remain in the evaluation range after the minimization, would be masked and not taken into account for further evaluation.

Figure 7 shows the surface of a tooth flank acquired by traversing the sensor in z -direction. As a result, the surface was measured by 3500 individual profile lines, which corresponds to 4.48 million measurement points. Hence, the linear scanning of the complete surface of a tooth flank is possible. Only in the root region at $x = 5$ mm, measurement artifacts are

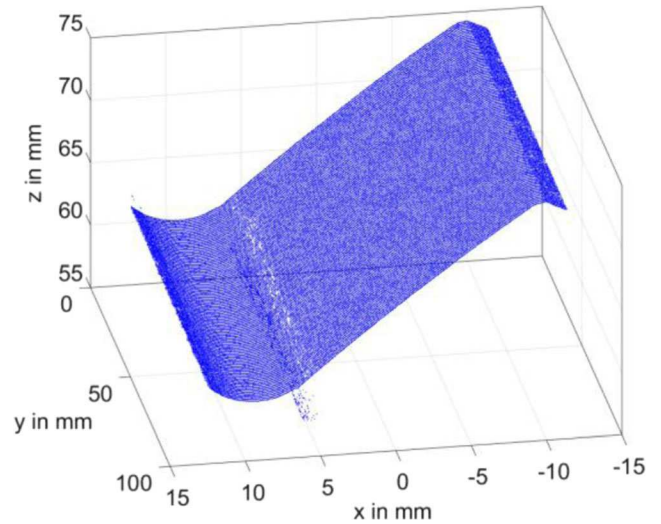


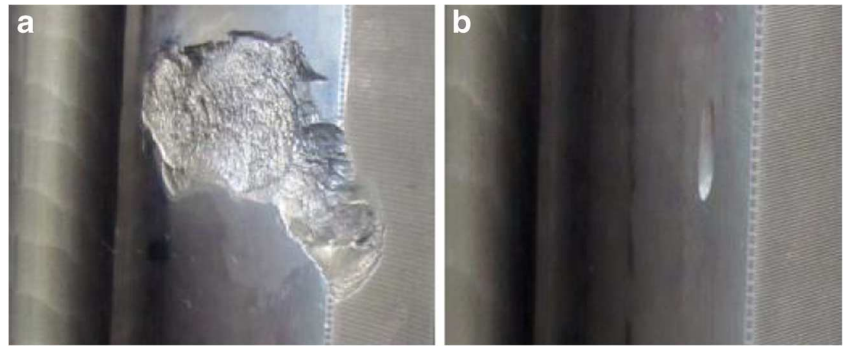
Fig. 7 Surface of one tooth flank of a large gear

visible due to multiple reflections. The complete scanning process takes 2 min. In a direct comparison, the measurement time for the tactile detection with the same point density would take 190 h. This demonstrates the considerable acceleration of an extensive measurement on large gears with the LLT with an acceleration factor of 5700. In terms of economic considerations, this acceleration can be applied to detect the surface of all tooth flanks of large gears three-dimensionally.

Due to the high and uniform number of measurement points on the entire surface, the surface of the tooth flank can be inspected along all three dimensions. For instance, surface defects such as breakouts and blemish (Fig. 8) can be detected quickly and automatically. Defects in form of breakouts and blemish usually occur during the operation of gearboxes and not in the production process. Figures 9 and 10 show the results of the linear scanning of the tooth flanks in the region of defects. The surface was detected with a high number of individual profile lines, which corresponds to about 640.000 measurement points. As result, the breakout and the blemish were resolved. In contrast to the insufficient information content from the tactile standard gear inspection, the detection probability of the defects is significantly higher with the fast optical 3D detection of the complete surface of a tooth flank.

As outlook, the detection of the total surface of the gearing can take place directly in the gearbox of a wind turbine without disassembling. Thus, any damage can be checked and monitored directly in the field of the environment. Therefore, the LLT has the potential for condition monitoring, e.g., in the operation of gearboxes in wind turbines. For the evaluation of the principle of laser triangulation for measurements on large gears in Section 4.2, the large gear from Table 1 is considered. On the basis of the chosen large gear, fundamental questions are examined for the acquisition and evaluation of the involute of the large gear with the LLT.

Fig. 8 Surface defects in form of breakouts (a) and blemish (b)



4.2 Evaluation and comparison with reference measurements

Figure 11 shows the result of the approximation of the measurement points to the nominal involute of the large gear. Thus, the measurement points from the LLT are transformed in the WCS (Fig. 11) of the gear based on the least squares sum of the orthogonal distances (Eq. 3). It should be noted that the evaluation is done for a single detected profile line (involute), with a static fixed positioning of the LLT sensor. In this case, the errors of the linear units can be neglected.

The result of the calculation of the orthogonal distance (d_i) of each aligned measurement point to the nominal involute of the gear is shown in Fig. 12. The orthogonal distances of each measurement point of the LLT and the reference measurement with the CMM are calculated with Eq. 3 within the WCS. The two curves in Fig. 12 indicate the deviation between the measured involutes and the nominal involute. The algebraic difference between the upper and the lower limit of the curve is the maximum measurement deviation. The maximal deviation of the LLT amounts to $\pm 10 \mu\text{m}$, whereas the deviation of tactile measurement is only $\pm 2.6 \mu\text{m}$. However, it must be taken into account that the measurements from the CMM are filtered, because the tactile ball probe of the CMM acts as a mechanical low-pass filter whose cut-off frequency is defined by the diameter of the ball probe [33, 34].

In order to specify the influence of the filter effect and the gear surface, the tooth surface was detected with a stylus

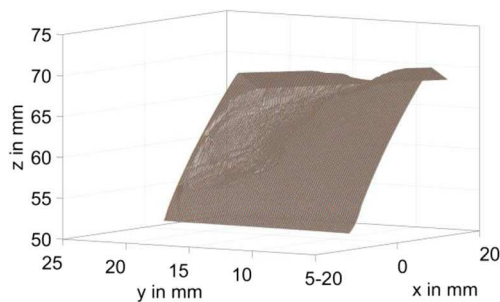


Fig. 9 Detection of a surface defect in form of a breakout as can be seen in Fig. 8a

instrument with a lateral resolution of $\leq 1 \mu\text{m}$. Thereby, the detected profile consists of form deviations, as well as waviness and roughness components. The evaluation of the measured values is carried out uniformly according to standards from the surface metrology. The roughness was not considered here, since the roughness value amounts to $R_a = 0.4 \mu\text{m}$ and can be neglected. The waviness height W_t is determined over ten measurements with a mean of $10.5 \mu\text{m}$, whereby the measurement distance l_n amounts to 12.5 mm . The waviness height for the LLT measurement is determined over ten measurements with a mean of $7.6 \mu\text{m}$. In the direct comparison, the evaluation of the CMM data has a waviness height of $4.6 \mu\text{m}$. Hence, the mechanical filter effect of the tactile ball probe [34] has a direct influence on the detection of the waviness height, and a large part of the waviness component is not detected with the tactile measurement. In proportion, the LLT is able to detect a large proportion of the waviness component of the surface. As result, the detection of the shape deviation by the LLT is one of the reasons for the high measurement deviation in direct comparison with the CMM data.

4.3 Measurement deviation

The measurement deviation of the LLT sensor can be divided into a random and a systematic part. For laser line triangulation, the speckle noise caused by the summation of light

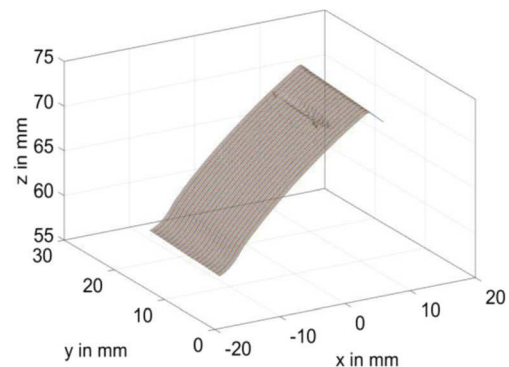


Fig. 10 Detection of a surface defect in form of a blemish as can be seen in Fig. 8b

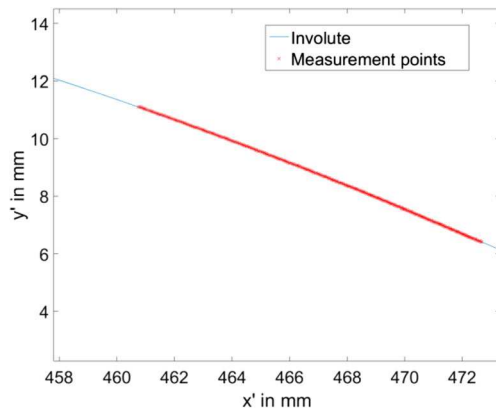


Fig. 11 Approximation of the measurement points (red dots) to the nominal involute (blue line) of the large gear within the WCS

waves with different phases on the CCD is typically one major source for the random error [27, 28]. The random error is defined by the fact that measured values are compared from different surfaces. The light waves may cancel or reinforce each other, leading to dark or bright speckles, respectively. The random process creates uncertainties in the determination of the exact centroid position of the CCD laser image, which is used to calculate the digitized coordinates [35]. The appearance of speckle depends on many parameters such as the temporal and spatial coherence of the illumination and the projection aperture, as well as the observation aperture of the sensor and the surface roughness [28]. The projection and observation aperture are fixed by the sensor. The roughness of the surface of the gear is defined by the manufacturing process. The change of the temporal coherence of the light source has not been carried out since it cannot be changed, because it is fixed by the commercial sensor. An extensive spatial incoherence in the luminous spot was also not investigated, because it has the consequence that the lateral resolution would be reduced [28], which is not desirable here.

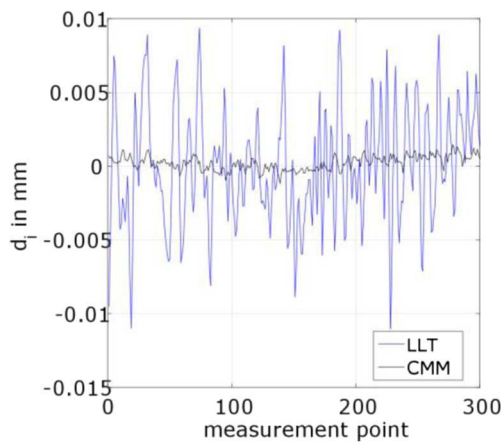


Fig. 12 Orthogonal distances (d_i) of each measurement point (LLT and CMM) to the involute

On the one hand, the systematic error is defined by the scanning depth and the projected angle of the LLT sensor. Since the triangulation angle is becoming smaller with an increasing scan depth, the standard deviation should rise with enlarging scan depth [35, 36]. On the other hand, the signal-to-noise ratio (SNR) must also be considered. In order to characterize the SNR of the sensor and the influence on the measurement deviation, the dynamic threshold of the sensor is varied in two steps (factor 4). The dynamic threshold refers to the evaluation of the intensity distribution (comparison of the gray value) of the sensor matrix, by applying a thresholding method for the segmentation procedure [37–39] and allows the segmentation of the exposed and the unexposed pixels. The method of the dynamic threshold determines a neighborhood N for each pixel, and calculates a suitable threshold value $t(N)$ based on this neighborhood whereby a dynamic adjustment is realized [38]. The dynamic threshold is insensitive to local brightness changes, e.g., reflections from the surface, thereby the illumination differences of the resulting image are balanced.

Figure 13 shows the result of the approximation of the measurement points to the nominal involute which are detected with a high dynamic threshold. The measurement points from the LLT are transformed into the WCS (Fig. 13) of the gear based on the least squares sum of the orthogonal distances (Eq. 3).

An increase of the dynamic threshold leads to a reduced number of measurement points. In addition, the higher threshold leads to an asymmetrical point distribution, whereby the point density in the root region is lower compared to the tip region (Fig. 13). The result of the calculation of the orthogonal distance d_i of each measurement point to the nominal involute of the gear can be seen in Fig. 14. This is done for a signal measurement (blue curve) and the mean of 100 measurements (red curve).

The increase of the dynamic threshold leads to an increase in the measurement deviation of the single measurement up to

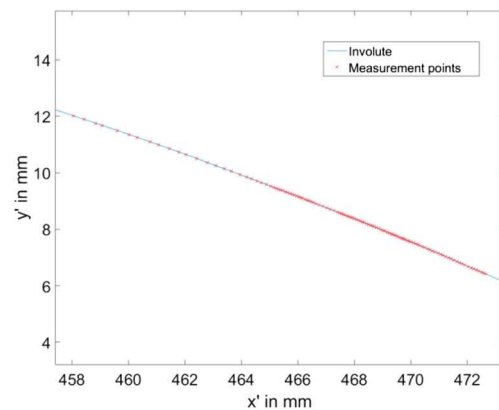


Fig. 13 Approximation of LLT measurement points (red), acquired with a high dynamic threshold, to the nominal involute (blue) of the large gear within the WCS

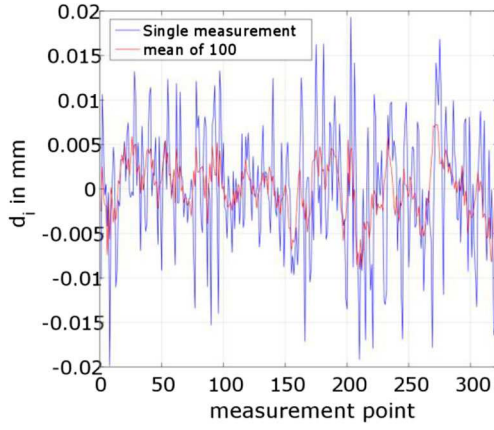


Fig. 14 Orthogonal distances from a single measurement (blue) and a mean of 100 measurements (red) to the nominal involute

$\pm 19.55 \mu\text{m}$. By calculating a temporal mean value from 100 measurements, the measurement deviation can be reduced to $8.2 \mu\text{m}$. Table 2 summarizes the measurement results with a low and a high threshold at given viewing angles.

Increasing of the dynamic threshold leads to a decrease in the number of measurement points (compare Table 2). As a result, a reduction in the point density has the consequence that in the approximation the weighting of a single measuring point increases. In addition, the relative noise in the image increases leading to an increased noise of the individual points.

The calculation of the mean value for a low dynamic threshold has no significant influence on the measurement deviation (italicized results in Table 2). In contrast to this, the determination of the mean value at a high dynamic threshold leads to a minimization of the measurement deviation (bold results in Table 2) between ± 7.55 and $\pm 8.2 \mu\text{m}$ which is dependent on the viewing angle. The reason is that a reduction of the noise component is realized by applying a time averaging of 100 measurements. As the noise arises stochastically, a summation of n measurements decreases the standard deviation of the noise signal by the factor \sqrt{n} [37, 40]. As result, the SNR increases by n with respect to the signal amplitudes. Since another increase in the dynamic threshold in combination with temporal averaging does not lead to a

further reduction in the measurement deviation, the measurement principle of the LLT is limited by the SNR. Hence, a measurement deviation of $\pm 8.2 \mu\text{m}$ can be achieved with the current measurement setup, which can be reduced in future investigations by minimizing the systematic errors.

5 Conclusion

The results at the tooth of the large cylindrical involute gear show the applicability of the laser line triangulation for the fast and multidimensional detection of the convex and reflective surface. In contrast to the tactile measurement technology, the laser line triangulation can detect 1280 measurement points simultaneously and has a measuring time of $< 10 \text{ ms}$. The high measurement rate is successfully applied in an optical scanning method for the three-dimensional measurement of a complete tooth flank. In direct comparison to tactile measurements on large gears, the laser line triangulation can considerably speed up the measurement with an acceleration factor of 5700. The fast and multidirectional detection of the complete surface of a tooth flank has advantages; thus, the detection of defects could take place directly in a gearbox. By that, damage occurring in the area of applications can be quantitatively and analyzed.

In order to minimize the systematic measurement deviations of $\pm 10 \mu\text{m}$, the dynamic threshold of the sensor has been increased. As a result, the number of measurement points decreased and the point distribution is asymmetrical and leads to an increase of the measurement deviation up to $\pm 19.55 \mu\text{m}$. However, temporal averaging at a high dynamic threshold leads to a minimization of the measurement deviation to $\pm 8.2 \mu\text{m}$. As result, the laser line triangulation on large cylindrical involute gears is limited by the SNR of the LLT sensor.

As outlook, the advantages such as measurement speed and the parallel data acquisition should be taken into account and implemented in the design of new

Table 2 Results of measurements with different viewing angles and dynamic thresholds

Dynamic threshold	Number of points	Single dev. in μm	Mean dev. in μm	Viewing angle in $^\circ$
Low	294	± 10.8	± 10.25	0
High	118	± 18.05	± 7.55	0
Low	380	± 9.3	± 9.05	10
High	268	± 21.55	± 7.80	10
Low	404	± 8.9	± 8.9	20
High	321	± 19.55	± 8.2	20

The italicized values show the calculation of the single and mean value for a low dynamic threshold.

optical sensor systems. To increase the resolution and to minimize the measurement uncertainty, an improved measurement arrangement would be if the sensor becomes smaller and could be placed within the gaps. In such a manner, the middle laser beam could be directed nearly perpendicular to the surface. However, this approach makes it difficult to implement a scanning measurement of all teeth. In order to realize a complete quality check of the gear, the presented measuring arrangement would have to be extended with a synchronized rotation axis, on which the gear is positioned. In such a setup, the currently unidentifiable quality parameters of the gear could be determined. Furthermore, the assessment of corresponding, multidimensional measurement strategies can only be carried out in the future with extended evaluation strategies, cf. [41], and 2D-filters for the optical measurement data.

Publisher's Note Springer Nature remains neutral with regard to jurisdictional claims in published maps and institutional affiliations.

References

- WindGuard (2016) Number of wind turbines in Germany
- Bauer E, Wikidal F, Gellermann T (2005) Überblick über Schäden am mechanischen Strang von Windenergieanlagen. In: Antriebstechnisches Kolloquium (ATK 2005), Aachen, pp 1–20
- Goch G (2003) Gear metrology. *CIRP Ann Manuf Technol* 52(2): 659–695. [https://doi.org/10.1016/S0007-8506\(07\)60209-1](https://doi.org/10.1016/S0007-8506(07)60209-1)
- Goch G, Knapp W, Härtig F (2012) Precision engineering for wind energy systems. *CIRP Ann Manuf Technol* 61(2):611–634. <https://doi.org/10.1016/j.cirp.2012.05.011>
- Härtig F, Rost K, Goch G (2010) Large gear material standard for the traceability of gears for transmission manufacturing. In: 4th International Conference on Gears, Garching, VDI-Berichte 2108: 991–1004
- ISO1328-1 (1995) Cylindrical gears - ISO system of accuracy - Part 1 Definitions and allowable values of deviations relevant to corresponding flanks of gear teeth
- Lu G, Wu S, Palmer N, Liu H (1998) Application of phase-shift optical triangulation to precision gear gauging. In: SPIE Proceedings Volume 3520:52–63. <https://doi.org/10.1117/12.334350>
- VDI/VDE 2607 (2000) Computer aided evaluation of profile and helix measurements on cylindrical gears with involute profile
- Härtig F, Lin H, Kniel K, Shi Z (2012) Standard conforming involute gear metrology using an articulated arm coordinate measuring system. *Meas Sci Technol* 23:105011. <https://doi.org/10.1088/0957-0233/23/10/105011>
- Franceschini F, Galetto M, Maisano D, Mastrogiacomo L (2016) Combining multiple large volume metrology systems: competitive versus cooperative data fusion. *Precis Eng* 43: 514–524. <https://doi.org/10.1016/j.precisioneng.2015.09.014>
- Schmitt RH, Peterek M, Morse E, Knapp W, Galetto M, Härtig F, Goch G, Hughes B, Forbes A, Estler WT (2016) Advances in large-scale metrology – review and future trends. *CIRP Ann Manuf Technol* 65(2):643–665. <https://doi.org/10.1016/j.cirp.2016.05.002>
- Petz M, Tutsch R, Christoph R, Andraes M, Hopp B (2012) Tactile–optical probes for three-dimensional microparts. *Measurement* 45:2288–2298. <https://doi.org/10.1016/j.measurement.2011.10.019>
- Gadelmawla ES (2011) Computer vision algorithms for measurement and inspection of spur gears. *Measurement* 44: 1669–1678. <https://doi.org/10.1016/j.measurement.2011.06.023>
- Balzer F, Schäfer M, Lindner I, Günther A, Stöbener D, Westerkamp J (2015) Recent advances in optical gear measurements - a new approach for fast measurements of large gears. In: 6th International Conference on Gears, Garching, VDI-Berichte 2255:655–666
- Meeß K, Kästner M, Seewig J (2006) Reduction and evaluation of the uncertainty of measurement of optical gear measurement using fringe projection. *tm – Technisches Messen* 73(11):603–610. <https://doi.org/10.1524/teme.2006.73.11.603>
- Fang S-P, Wang L-J, Komori M, Kubo A (2011) Design of laser interferometric system for measurement of gear tooth flank. *Optik* 122:1301–1304. <https://doi.org/10.1016/j.ijleo.2010.09.002>
- Yang HZ, Qiao XG, Luo D, Lim KS, Chong W, Harun SW (2014) A review of recent developed and applications of plastic fiber optic displacement sensors. *Measurement* 48:333–345. <https://doi.org/10.1016/j.measurement.2013.11.007>
- Lyda W, Gronle M, Fleischle D, Mauch F, Osten W (2012) Advantages of chromatic-confocal spectral interferometry in comparison to chromatic confocal microscopy. *Meas Sci Technol* 23: 054009. <https://doi.org/10.1088/0957-0233/23/5/054009>
- Trocha P, Karpov M, Ganin D, Pfeiffer MH, Kordts A, Wolf S, Krockenberger J, Marin-Palomo P, Weimann C, Randel S (2018) Ultrafast optical ranging using microresonator soliton frequency combs. *Science* 359:887–891. <https://doi.org/10.1126/science.aao3924>
- Katsuhiko Miura TT, Nose A, Takeda R, Ueda S (2018) Accuracy verification of gear measurement with a point autofocus probe. In: euspen's 18th International Conference and Exhibition, pp 121–122
- Wu S, Lu G (1998) Non-contact, high-speed, precision gear inspection. In: AHS International Annual Forum, Washington (DC), pp 701–711
- Younes MA, Khalil AM, Damir MN (2005) Automatic measurement of spur gear dimensions using laser light, part 2: measurement of flank profile. *Opt Eng* 44:103603. <https://doi.org/10.1117/1.2114987>
- Chow J, Xu SLT, Kengkool K (2002) Development of an integrated laser-based reverse engineering and machining system. *Int J Adv Manuf Technol* 19(3):186–191
- Zhang S (2010) Recent progresses on real-time 3D shape measurement using digital fringe projection techniques. *Opt Lasers Eng* 48:149–158. <https://doi.org/10.1016/j.optlaseng.2009.03.008>
- Xiao Y-L, Su X, Chen W, Liu Y (2012) Three-dimensional shape measurement of aspheric mirrors with fringe reflection photogrammetry. *Appl Opt* 51:457–464. <https://doi.org/10.1364/AO.51.000457>
- Peggs GN, Muralikrishnan B, Ziebart M, Robson S, Forbes AB, Hughes EB, Maropoulos PG (2009) Recent developments in large-scale dimensional metrology. *Proc Inst Mech Eng B J Eng Manuf* 223:571–595
- Baribeau R, Rioux M (1991) Influence of speckle on laser range finders. *Appl Opt* 30:2873–2878. <https://doi.org/10.1364/AO.30.002873>
- Dorsch RG, Häusler G, Herrmann JM (1994) Laser triangulation: fundamental uncertainty in distance measurement. *Appl Opt* 33: 1306–1314. <https://doi.org/10.1364/AO.33.001306>

29. Günther A, Peters J, Goch G (2001) Areal numerical description, alignment and evaluation of cylindrical gears. *tm – Technisches Messen* 68(4):160–165. <https://doi.org/10.1524/teme.2001.68.4.160>
30. Stöbener D, von Freyberg A, Fuhrmann M, Goch G (2012) Areal parameters for the characterisation of gear distortions. *Materialwissenschaft und Werkstofftechnik* 43(1–2):120–124. <https://doi.org/10.1002/mawe.201100898>
31. Stöbener D, von Freyberg A, Fuhrmann M, Goch G (2011) Characterisation of gear distortions with areal parameters. In: Zoch HW, Lübben T (eds) 3rd International Conference on Distortion Engineering, pp 147–154
32. Grubbs FE (1969) Procedures for detecting outlying observations in samples. *Technometrics* 11(1):1–21. <https://doi.org/10.2307/1266761>
33. Lonardo PM, Lucca DA, De Chiffre L (2002) Emerging trends in surface metrology. *CIRP Ann Manuf Technol* 51(2):701–723. [https://doi.org/10.1016/S0007-8506\(07\)61708-9](https://doi.org/10.1016/S0007-8506(07)61708-9)
34. Weckenmann A, Estler T, Peggs G, McMurtry D (2004) Probing systems in dimensional metrology. *CIRP Ann Manuf Technol* 53(2):657–684. [https://doi.org/10.1016/S0007-8506\(07\)60034-1](https://doi.org/10.1016/S0007-8506(07)60034-1)
35. Feng H-Y, Liu Y, Xi F (2001) Analysis of digitizing errors of a laser scanning system. *Precis Eng* 25:185–191. [https://doi.org/10.1016/S0141-6359\(00\)00071-4](https://doi.org/10.1016/S0141-6359(00)00071-4)
36. Van Gestel N, Cuypers S, Bleys P, Kruth J-P (2009) A performance evaluation test for laser line scanners on CMMs. *Opt Lasers Eng* 47: 336–342. <https://doi.org/10.1016/j.optlaseng.2008.06.001>
37. Gonzalez RC, Woods RE (2018) *Digital image processing*. 4th ed. Pearson, New Jersey, pp 804–825
38. Jähne B (2005) *Digital image processing*, 6th ed. Springer, pp 449–462
39. Kang S-D, Yoo H-W, Jang D-S (2007) Color image segmentation based on the normal distribution and the dynamic thresholding. In: *Computational science and its applications – ICCSA, Kuala Lumpur*, pp 372–384
40. Kay SM (1993) *Fundamentals of statistical signal processing*, Prentice Hall, pp 27–81
41. Goch G, Ni K, Peng Y, Guenther A (2017) Future gear metrology based on areal measurements and improved holistic evaluations. *CIRP Ann Manuf Technol* 66(1):469–474. <https://doi.org/10.1016/j.cirp.2017.04.046>